Gyrotron Internal Mode Converter Reflector Shaping from Measured Field Intensity

Denison, D. R., Chu, T. S.*, Shapiro, M. A., Temkin, R. J.

December 1998

Plasma Science and Fusion Center
Massachusetts Institute of Technology
Cambridge, MA 02139

Abstract

We present the formulation and experimental results of a new approach to designing internal mode converter reflectors for high-power gyrotrons. The method employs a numerical phase retrieval algorithm that reconstructs the field in the mode converter from intensity measurements, thus accounting for the true field structure in shaping the beam-forming reflectors. An outline for designing a four-reflector mode converter is presented and generalized to the case of an offset-fed shaped reflector antenna. The requisite phase retrieval and reflector shaping algorithms are also developed without reference to specific mode converter geometry. The design approach is applied to a 110 GHz internal mode converter that transforms the $TE_{22,6}$ gyrotron cavity mode into a Gaussian beam at the gyrotron window. Cold test experiment results of the mode converter show that a Gaussian beam with the desired amplitude and phase is formed at the window aperture. Subsequent high-power tests in a 1 MW gyrotron confirm the Gaussian beam observed in cold tests. The general development of the approach and its validation in a quasi-optical mode converter indicate that it is also applicable to other quasi-optical, microwave applications such as radio astronomy, free-space transmission lines, and mitre bends for overmoded waveguides.

*Microwave Power Products Division, Communications and Power Industries, Palo Alto, CA 94303 USA

1 Introduction

Gyrotron internal mode converters transform the high-order circular waveguide mode of a gyrotron cavity into a Gaussian-like mode suitable for free-space propagation. A typical mode converter consists of a waveguide section with a radiating aperture followed by a series of reflectors (or mirrors), as depicted in Figure 1. The waveguide constitutes either a Vlasov [1] or rippled-wall [2] launcher that directs the microwave energy radially through a wall aperture, separating it from the spent electron beam. The radiated wave is then focussed by a series of reflectors that also serve to guide the microwave beam through a low-loss vacuum window and out of the tube.

At the power levels of microwave radiation produced by conventional high-power ($\sim$ 1 MW) gyrotrons, the electric field intensity profile over the window aperture proves to be the limiting factor in the overall power handling capability of the gyrotron for long-pulse and CW operation. The microwave beam shape on the window is constrained by the thermal characteristics of the window material and cooling configuration, as well as by edge diffraction losses at the window aperture. The internal mode converter reflectors must be shaped to provide a field profile at the window that accommodates the thermal properties of the window material and minimizes edge losses.

Previous mode converter reflector designs have relied on numerical simulations of the fields radiated by the launcher. For instance, the rippled-wall launcher can be modeled using coupled mode theory, which leads to a set of simultaneous differential equations that are solved numerically for the fields inside the guide [3]. The radiated field, computed from a vector diffraction integral, behaves as a quasi-Gaussian beam that can be focussed into a nearly-ideal Gaussian beam at the window by using doubly-curved reflectors designed from analytic expressions [3, 4]. For more complicated final beam shapes, such as a flat power profile over the window aperture, reflector synthesis methods that incorporate the simulated launcher fields in the reflector shaping are used [5]. Experimental results have demonstrated, however, that the field intensity on the gyrotron window often does not agree with the design profile [6]. This deviation from design results in a lower power handling capability of the window, limiting the overall performance of the gyrotron.
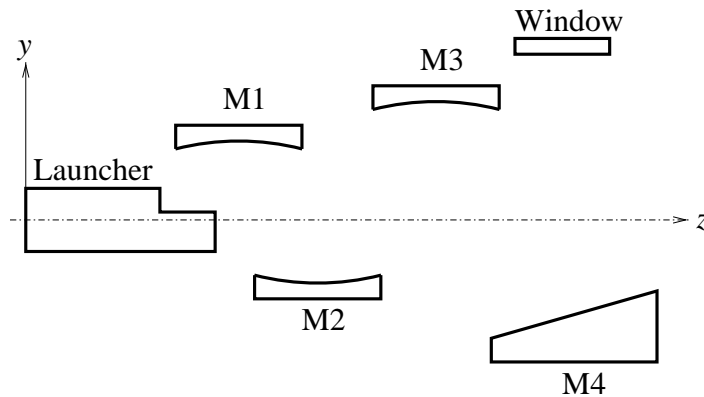

Figure 1: Mode Converter Schematic.

Cold test (low-power) measurements of the field profile in the mode converter reveal that the fields radiated by the launcher differ from those predicted by theory. This difference may arise from machining errors in the launcher, misalignment of the launcher with respect to the reflectors, or an incomplete theory for the launcher. Such variations from the ideal, theoretical situation suggest that any reflector design based on simulated fields will not produce the desired output field in actual operation. In order to overcome the observed difficulties in forming the desired microwave beam shape in a gyrotron, we recently proposed a new approach to reflector design that incorporates measured field intensities in the design process [7].

The following paper reports the development and experimental validation of this approach to internal mode converter reflector design. Section 2 outlines the basic design procedure for a four-reflector internal mode converter. The reflectors are treated as phase-correcting surfaces, which permits a generalization of the design approach to arbitrary quasi-optical systems. An algorithm for retrieving phase from intensity measurements is discussed in Section 3, while Section 4 extends the phase retrieval algorithm to the problem of shaping phase-correcting surfaces. Section 5 applies the proposed design method to a 110 GHz internal gyrotron mode converter with a diamond window. We present experimental results for both cold tests and hot tests that verify the efficacy of the proposed method.

2 Outline of Reflector Design Approach

As discussed in Section 1, the measured output beam of gyrotron mode converters often differs from the theoretically-predicted fields. This discrepancy between theory and experiment appears to originate with the launcher fields. For example, consider a 110 GHz gyrotron internal mode converter that uses a rippled-wall launcher and four reflectors (Figure 1) to transform the $TE_{22,6}$ cylindrical mode into a flat-top beam at the output window. Figure 2 shows the theoretically-computed field intensity at the plane of the third reflector surface (M3 in Figure 1), while Figure 3 gives the measured field intensity over the same plane. In each figure, the z-axis origin is at the beginning of the launcher, as depicted in Figure 1. Although the two patterns are similar, there are significant differences in the size and shape of the individual intensity contours that ultimately result in the observed differences between theoretical and experimental window electric field intensity profiles [6].

To account for the actual fields in the mode converter, we propose the following procedure for designing the reflectors based on intensity measurements [7, 8]:

1. Design and build the launcher to produce a Gaussian-like beam.

2. Measure the field radiated by the launcher and design the first doubly-curved reflector by fitting an elliptical Gaussian beam to the measured pattern.

3. Measure the field intensity following the first reflector and design the second reflector based on a best-fit Gaussian.

4. Measure the field intensity following the second reflector and retrieve the phase of the beam to reconstruct the full field structure of the wave.
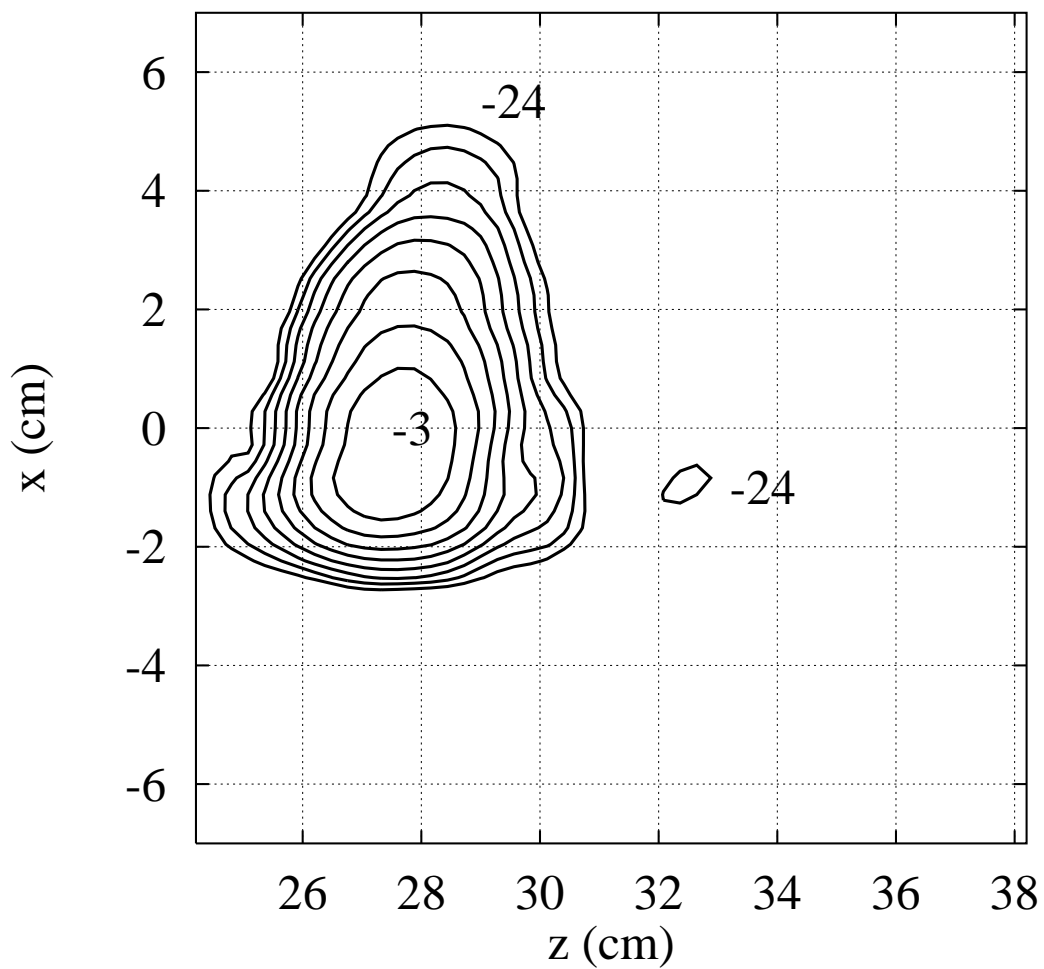
Figure 2: Theoretical field intensity over a plane at the Reflector 3 position. Contours of constant $|E_x|^2$ are at 3 dB intervals from peak; the -3 dB and -24 dB curves are labeled.
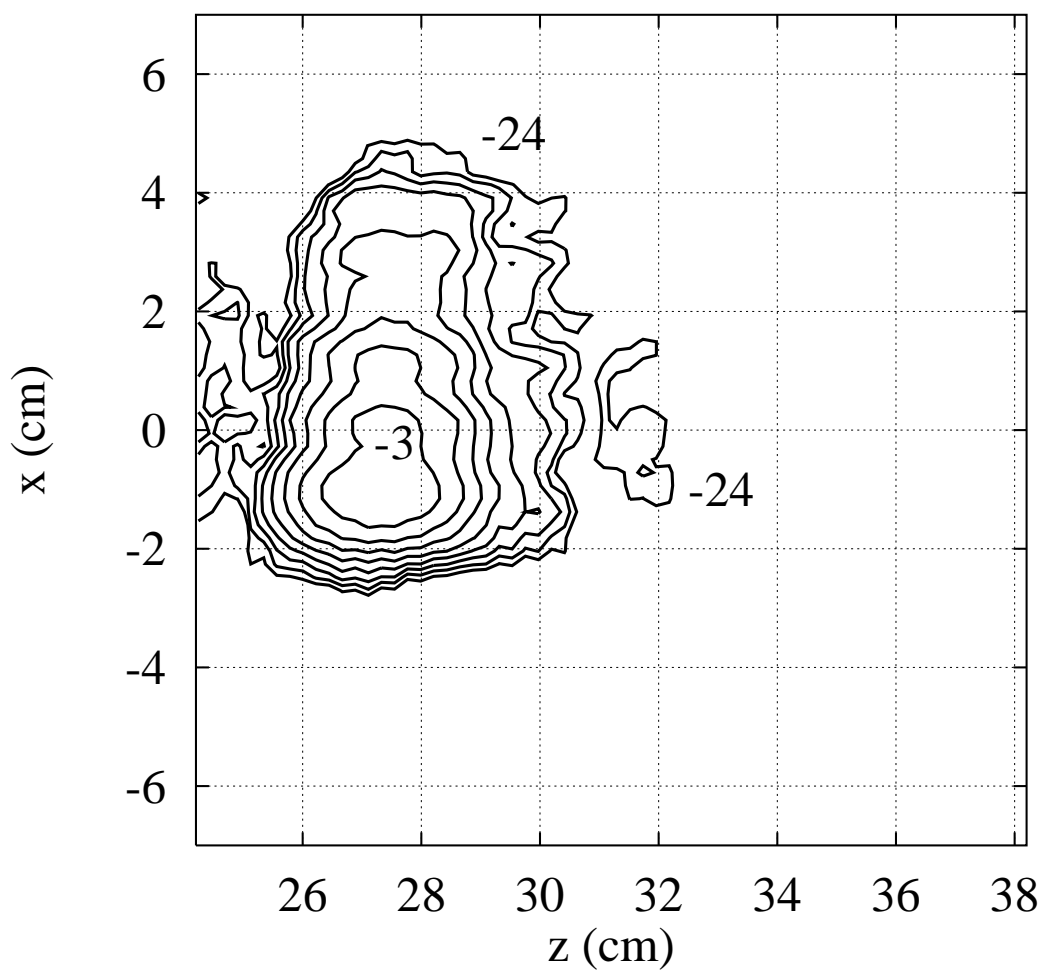
Figure 3: Measured field intensity over a plane at the Reflector 3 position. Contours of constant $|E_x|^2$ are at 3 dB intervals from peak; the -3 dB and -24 dB curves are labeled.

5. Use the reconstructed field after the second reflector and the desired field structure on the window as input to a reflector shaping procedure to determine the surface profiles for reflectors three and four.

6. Simulate reflectors three and four in a numerical electromagnetics code to verify the design.

These steps can be generalized to the case of shaping reflectors in an offset-fed, dual-reflector antenna. Steps (1) – (3) define the feed, and the remaining steps involve shaping the reflector antennas from measurements of the feed. The above outline then reduces to the problems of retrieving phase from intensity measurements and reflector shaping.

3   Phase Retrieval from Intensity Measurements

At high frequencies (> 100 GHz), the difficulties of directly measuring phase lead to the stipulation that we recover the phase from field intensity measurements. This phase retrieval problem was considered by Katsenelenbaum [9] in terms of an iterative determination of phase correctors; Gerchberg and Saxton [10] (evidently independently) introduced a similar approach for the more restrictive case of retrieving phase from an object function and its Fourier transform. The general case of two or more arbitrary measurement planes is presented as a modified Gerchberg-Saxton algorithm by Anderson and Sali [11], and we outline a similar method below. Although the formulation is in terms of a scalar field, we can always decompose the beam in free space as a sum of three linear field vectors. The additional issues of attainability, uniqueness, convergence of the solution, and experimental validation of this inverse problem have been the subject of much study; for a survey see [9] – [16].

Iterative phase retrieval is accomplished with the following algorithm. Suppose we have two measurement planes, perpendicular to the z-axis in a Cartesian coordinate system, with a wave propagating roughly paraxially, or quasi-optically, along the z-axis. The measurement planes are located at z_1 and z_2 with $z_1 < z_2$, and the (for now continuous) measured amplitude over each plane is denoted $A_1(x,y)$ and $A_2(x,y)$, respectively.

The total scalar fields on the two measurement planes are then written as

$$u_1(x,y,z_1) = A_1(x,y)e^{i\phi_1(x,y)} \qquad u_2(x,y,z_2) = A_2(x,y)e^{i\phi_2(x,y)}, \qquad (1)$$

where $\phi_1(x,y)$, $\phi_2(x,y)$ are the exact phases on their respective planes. The fields are related by the plane wave expansion as

$$u_2(x,y,z_2) = \mathcal{F}^{-1}\left\{ e^{i(z_2-z_1)\sqrt{k^2-k_x^2-k_y^2}} \cdot \mathcal{F}\left\{u_1(x,y,z_1)\right\}\right\}, \qquad (2)$$

where $\mathcal{F}$ is the Fourier transform and $\mathcal{F}^{-1}$ its inverse. Our earlier requirement that the beam propagate roughly paraxially stems from the fact that in the case of discretely sampled data under practical measuring conditions, the range in k-space for the Fourier kernel is limited by the sampling rate, and we cannot hope to recover modal components of the wave that have large values of k_x and k_y. Furthermore, we plan to treat the reflectors as

phase-correcting surfaces in Section 4, and that decision necessarily limits our approach to quasi-optical beams.

The phase is retrieved by iteratively solving (2) for the phase functions ϕ_1, ϕ_2 with the measured amplitudes as weights. For compactness, we have dropped the explicit variable dependence in the field functions u, A, and ϕ. Beginning with an initial phase guess on the first plane, $\phi_1^{(0)}$, we compute $u_2^{(0)}$ with $u_1^{(0)} = A_1 e^{i\phi_1^{(0)}}$, where the superscript denotes the field after the nth iteration. Clearly, the calculated amplitude on plane 2, $A_2^{(0)}$, will not equal the measured (correct) amplitude over that plane (unless the initial phase guess was the actual phase on plane 1). We can represent the error after each iteration as

$$E_{1,2}^{(n)} = \int_{S_{1,2}} |A_{1,2} - A_{1,2}^{(n)}|^2 dS_{1,2}, \tag{3}$$

where the subscripts 1, 2 refer to the corresponding plane.

For the next stage of the iteration, we replace the computed amplitude on plane 2 with the measured amplitude A_2 to produce a modified field on plane 2: $u_2^{(0)} = A_2 e^{i\phi_2^{(0)}}$. We then propagate this field back to plane 1 via (2), with indexes 1 and 2 interchanged. A new field is constructed on plane 1 using the computed phase and measured amplitude on that plane. The process is repeated N times until the error $E^{(N)}$ (3) is less than some prescribed value.

The advantage of the above phase retrieval algorithm lies in evaluating (2) for the case of discretely-sampled amplitudes (or field intensity I, where $A = \sqrt{I}$). Each iteration involves two discrete Fourier transforms and one complex multiply. Using a two-dimensional Fast Fourier transform [17] we can rapidly compute (2). We have implemented this approach in an original FORTRAN code that has been benchmarked against simulated and measured data. In practice, the error (3) tends to decrease in stages with a number of plateaus before the error reaches some absolute minimum (see e.g. [13]). Our studies of simulated data indicate that overcoming the local minima corresponds to improving the resolution of fine details of the field structure, particularly at low intensity. Additionally, the convergence of the solution depends on the distance between measurement planes, with larger plane separations improving the rate of convergence. However, if the beam changes significantly over a relatively short distance, then the measurement data still contain sufficient information for the phase retrieval, at the expense of needing more iterations. Given these factors, the ability to perform many (100 – 1000) iterations, made feasible by our implementation of the phase retrieval algorithm, is crucial to obtaining an accurate field reconstruction.

4   Reflector Shaping

In Section 2 we introduced the concept that the launcher and first two reflectors in the mode converter constitute a feed in a conventional offset-fed, dual-reflector antenna. Extending this analogy, we can view the shaping of reflectors three and four as the general problem of beam synthesis in antenna design — given a specified feed, shape the reflectors to produce the desired output beam.

$$\Delta_1 \qquad\qquad \Delta_2$$

$$Ae^{i\,\varphi_1} \qquad Ae^{i\,\varphi_1^{sc}} \qquad Ae^{i\,\varphi_2^{sc}} \qquad Ae^{i\,\varphi_2}$$
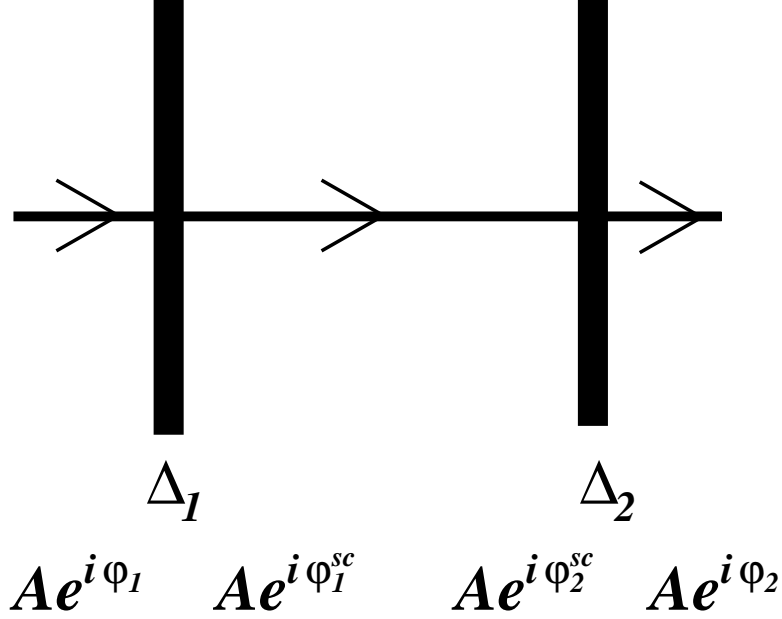
Figure 4: Reflector shaping geometry.

One technique for shaping the reflectors is to treat them as phase-correcting surfaces; that is, the polarization and amplitude of the incident wave remain unchanged upon reflection. This approximation holds for a wide class of quasi-optical microwave engineering problems; the design of mirrors, lenses, and resonators in Gaussian optics relies heavily on modeling elements as phase correctors (e.g. [4]). Another advantage of this treatment is that we can use the phase retrieval algorithm described in Section 3 to define the phase correcting surfaces [18, 19, 20], unifying our design approach under a single construct.

To see the relationship between phase retrieval and reflector shaping, consider the geometry of Figure 4. The two phase-correcting surfaces are cast as equivalent thin lenses with phase-correcting functions $\Delta_1(x,y)$ and $\Delta_2(x,y)$. The beam is propagating along the z-axis, perpendicularly to each lens surface. The incident beam is denoted as $A_1 e^{i\phi_1}$ and the output beam is $A_2 e^{i\phi_2}$. We see that the amplitudes A_1 and A_2 may be associated through the pair of self-consistent phases ϕ_1^{sc} and ϕ_2^{sc}, which are determined by applying the phase retrieval algorithm to A_1 and A_2. Then the phase correcting function required to transform the incident phase, ϕ_1, into the first self-consistent phase, ϕ_1^{sc}, is given by $\Delta_1 = \phi_1^{sc} - \phi_1$. Similarly for the second phase-correcting function we have $\Delta_2 = \phi_2 - \phi_2^{sc}$.

In the above procedure we see that the first phase corrector transforms the incident phase such that the beam amplitude at the second phase corrector will be the desired output amplitude, A_2, and the second corrector synthesizes the desired output phase. An interesting consequence of this observation is that we can produce a specified beam intensity, but not phase, using only one reflector. This situation is related to basic Gaussian optics where we can use a single spherical mirror or lens to transform a Gaussian beam into either a beam with a specified waist size or with a specified minimum waist position (focal length), but not both.

5 Experimental Results for a 110 GHz Gyrotron

5.1 Overview

Our application involves retrofitting the last two reflectors (M3 and M4 in Figure 1) of the existing mode converter in a 1 MW, 110 GHz gyrotron. The existing mode converter transforms the $TE_{22,6}$ cavity mode into a beam with a flat power profile across a 10-cm-diameter double-disk sapphire window. The new mode converter uses a 5-cm-diameter diamond window to improve the power-handling capabilities of the gyrotron, and new mode converter reflectors are required to produce a Gaussian beam on the window. The specified beam minimum waist is 1.52 cm and should occur at the window aperture, providing a flat phase over the window. This waist size corresponds to a theoretical transmission of 99.6% of the power in the microwave beam through the window aperture. These requirements of circular beam shape, flat phase, and high transmission efficiency at the window are stringent, and they provide a rigorous test of the proposed reflector design.

5.2 Feed Field Measurements

The first two reflectors in the mode converter were previously designed as toroidal (doubly-curved) surfaces based on simulated fields from the launcher, obviating the need in this application for Steps (1) – (3) in Section 2. The pre-existing launcher and toroidal reflectors thus form a feed whose radiated field we measure according to Step (4).

The feed field intensity measurements were performed at Communications and Power Industries (CPI) using a three-axis motorized scanner built by the University of Wisconsin [5]. The receiving horn was an open-ended waveguide mounted on the scanner and fed to a heterodyne receiver. The feed structure was placed external to the gyrotron tube and the scanner was oriented to make planar scans as shown in Figure 5. The launcher was excited by a Gunn diode source whose output was transformed into the $TE_{22,6}$ mode by a coaxial mode transducer. The mode purity of this transducer is estimated to be approximately 99 %; a detailed discussion of mode purity in a similar transducer designed for the $TE_{15,2}$ mode is given in [21].

We performed measurements over nine planes near the position of the third reflector, as shown schematically in Figure 5. The planes are 14 cm × 14 cm with a 64 point × 64 point sampling grid that corresponds to a sampling density of 0.8λ. Figure 3 shows the measured field intensity on the plane of the third reflector, and Figure 6 shows the measured field intensity 11.9 cm from the third reflector plane. The beam is propagating paraxially along a line 25° off the y-axis, out of the page, and has < -25 dB cross-polarization, indicating the scalar phase retrieval is suitable for this case. Furthermore, the beam shape changes significantly over the measurement range — from Figure 3 to Figure 6 —, so despite our relatively close plane spacing (on the order of tens of wavelengths) we can still expect an accurate field reconstruction according to the discussion in Section 3.
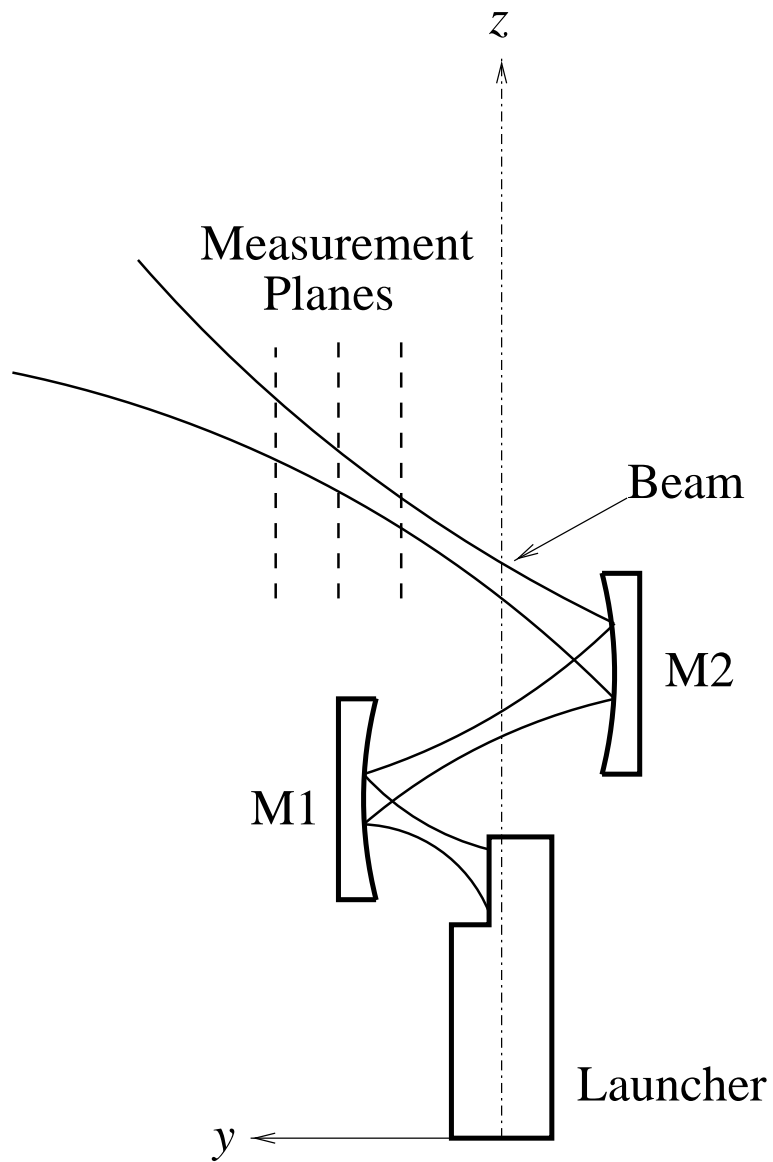
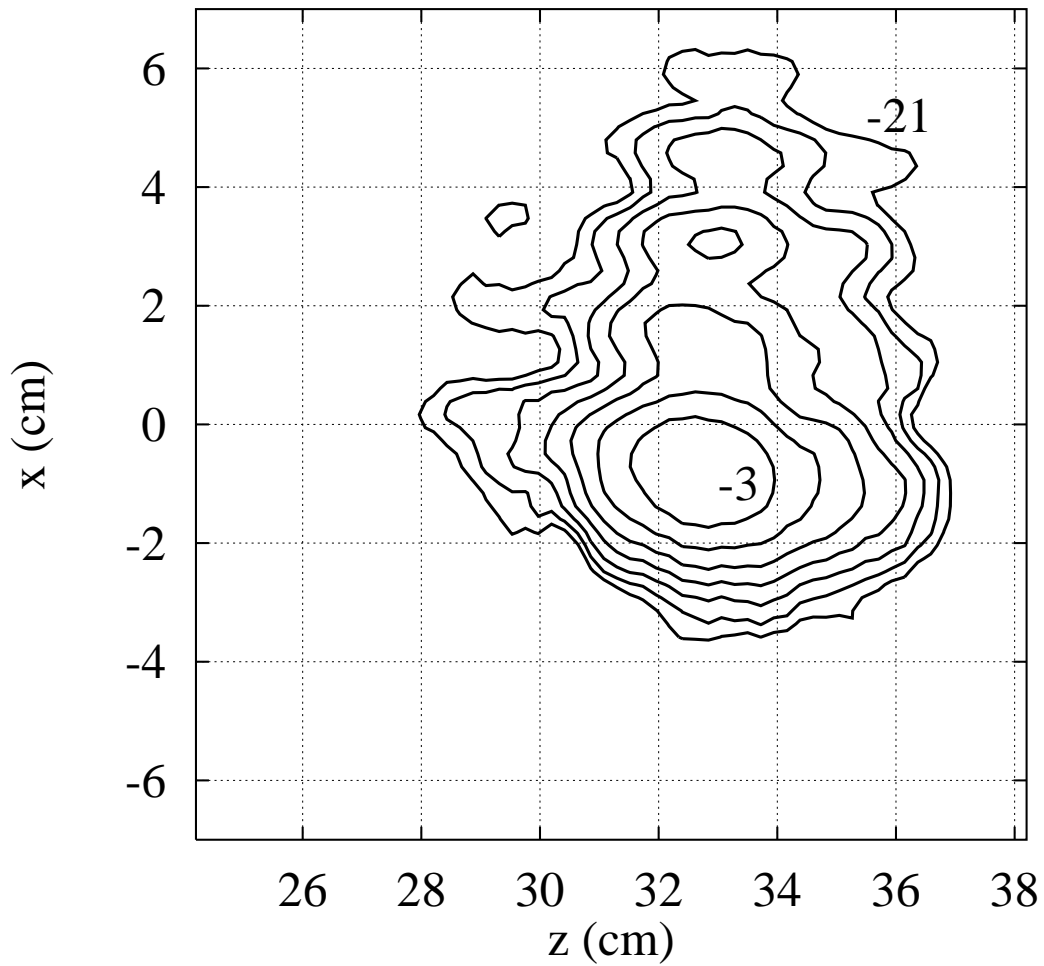Figure 5: Schematic of scan geometry for the rigid launcher-toroidal reflector feed structure.

Figure 6: Measured field intensity on a plane located 11.9 cm in y from the Reflector 3 position. Contours of constant $|E_x|^2$ are at 3 dB intervals from peak; the -3 dB and -21 dB curves are labeled.

5.3 Phase Retrieval

The measurements detailed in Section 5.2 were interpolated onto 128 point × 128 point grids to provide a 0.4λ grid spacing in order to avoid half-wavelength undersampling numerical artifacts in the phase retrieval. In addition, we modified the beam shape and position to temporarily create a beam propagating normal to the measurement (or observation) planes. Specifically, the profile of the beam was contracted by a factor $\cos\theta$ in z (θ is the incidence angle with respect to the plane normal) to account for the beam distension over the measurement planes, and the geometric centers of the beams were aligned along a common propagation axis. Such a transformation relieves the phase retrieval algorithm of retrieving both the nominal phase structure and phase tilt of the beam. Oblique beam propagation is accomplished by adding a phase tilt a posteriori to the nominal phase structure determined by the phase retrieval.

The phase was retrieved in 500 iterations with three measurement planes located approximately 25λ apart. The reconstructed field was propagated to an independent (i.e. not used in the reconstruction) measurement plane to verify the phase retrieval, and we observed good agreement between the measured and simulated amplitudes on that plane.

5.4 Reflector Shaping and Simulation

We shaped a pair of reflectors using the procedure described in Section 4 with the reconstructed field from Section 5.3 as the incident wave, $A_1 e^{i\phi_1}$, and the desired Gaussian as output, $A_2 e^{i\phi_2}$.

One important aspect of the reflector shaping procedure not mentioned in Section 4 is the fact that the physical sizes of the actual reflector surfaces must be taken into account in the shaping. For instance, the third reflector (M3 in Figure 1) is limited in z — along the tube axis — to approximately 8.5 cm; this dimension is large enough to intercept both the main beam and the -24 dB sidelobe in Figure 3, but it is significantly more narrow than the observation plane. To account for the smaller size of the physical surface, we simply set all field amplitudes outside of the surface perimeter to zero. The benefit of incorporating the final reflector dimensions in the shaping procedure becomes apparent if we consider instead the case of using the whole observation plane in the design and then forming the surface boundary afterwards. The result is that our assumed field over the entire observation plane will be truncated by a rectangular window whose pulse width is the physical width of the reflector. The radiated field reveals this windowing as the familiar convolution of the desired field pattern with a sinc function, which leads to unwanted sidelobes.

The final reflector surface shapes are shown in Figure 7. For the third reflector, the beam is incident from below. Physically, we see that the elongation in the x-direction of the pattern in Figure 3 will be focussed into the main portion of the beam by the sharp curvature evident for $x > 0$ in the reflector's profile. The random surface fluctuations around the edge of the reflector arise because the phase in that negligible-amplitude region is indeterminate. The beam radiated from the third reflector propagates to the fourth reflector, also shown in Figure 7. The surface is strongly spherical to focus the incident wave into the desired Gaussian beam at the window aperture.

The reflectors were simulated in a physical optics code [3] using the reconstructed feed
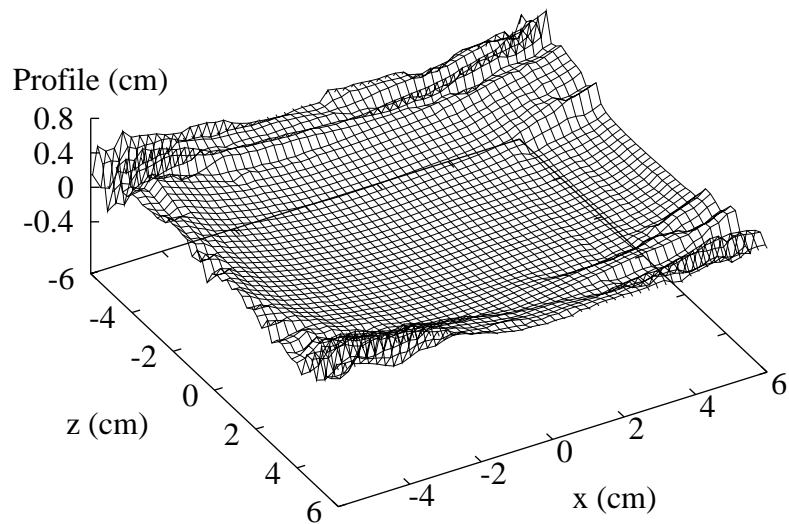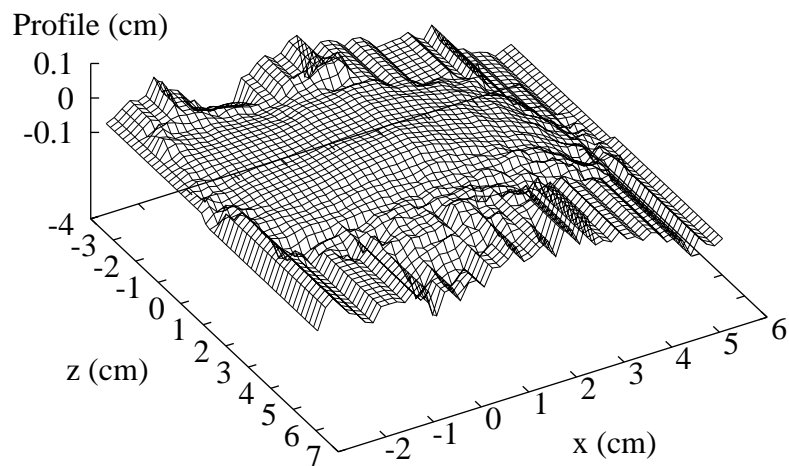
12

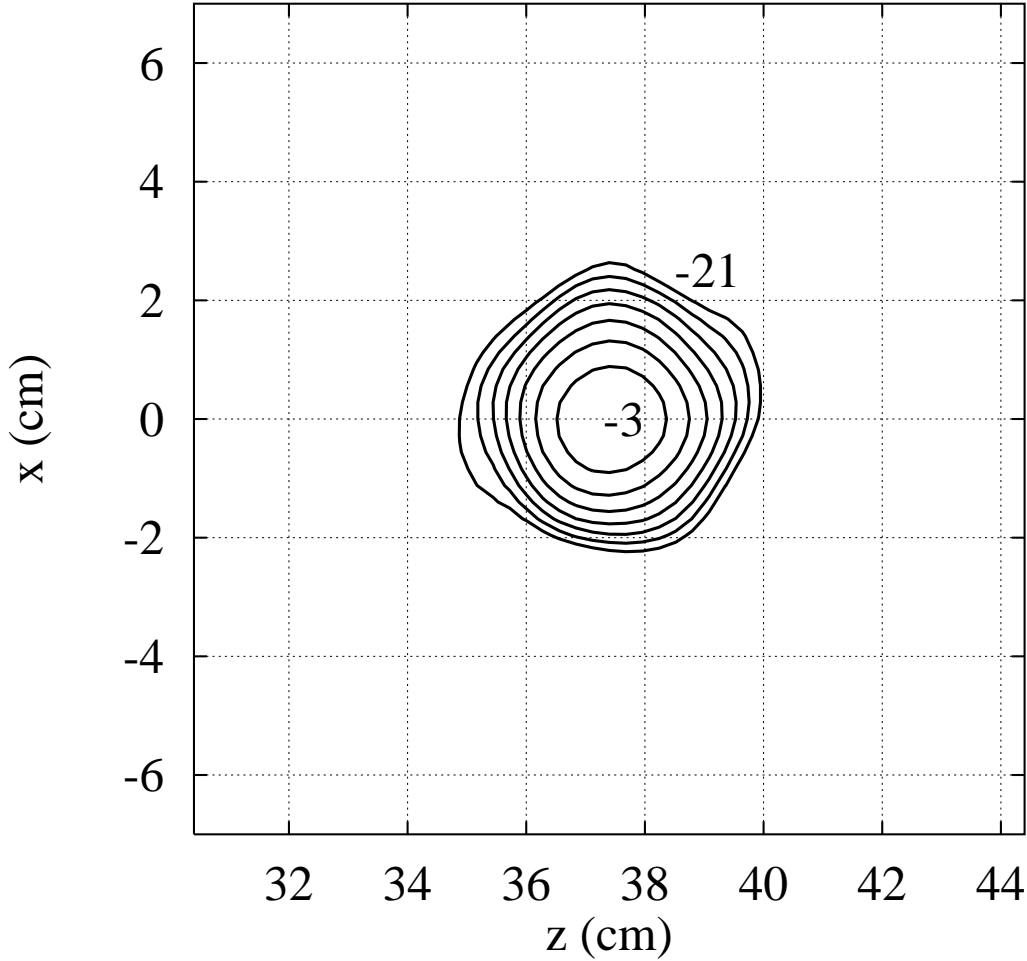Figure 7: Top: Third reflector profile. Bottom: Fourth reflector profile.

Figure 8: Simulated field intensity on the window plane. The window center is at $z = 37.4$ cm, $x = 0$ cm. Contours of constant $|E_x|^2$ are at 3 dB intervals from peak; the -3 dB and -21 dB curves are labeled.

fields as the initial field distribution. The physical optics code is independent of the code used in the phase retrieval/reflector shaping, and thus will reveal any systemic errors (if they exist) in the phase retrieval code. The simulated field intensity pattern on the window, shown in Figure 8, is in fact the desired Gaussian beam. Integrating the power over the observation plane reveals that 99.5% of the beam power will pass through the aperture as compared to 99.6% for an ideal Gaussian with a waist size of 1.52 cm in the 5 cm aperture. Figure 9 compares the intensity profile of the desired Gaussian beam to the simulated beam. The simulated beam exhibits a nearly-ideal Gaussian profile with a waist size of 1.55 cm — 0.03 cm larger than the 1.52 cm design. The sidelobe to the right of beam, on the $+z$ side, corresponds to unrecovered sidelobe power originally generated by the feed, as seen in Figure 3.
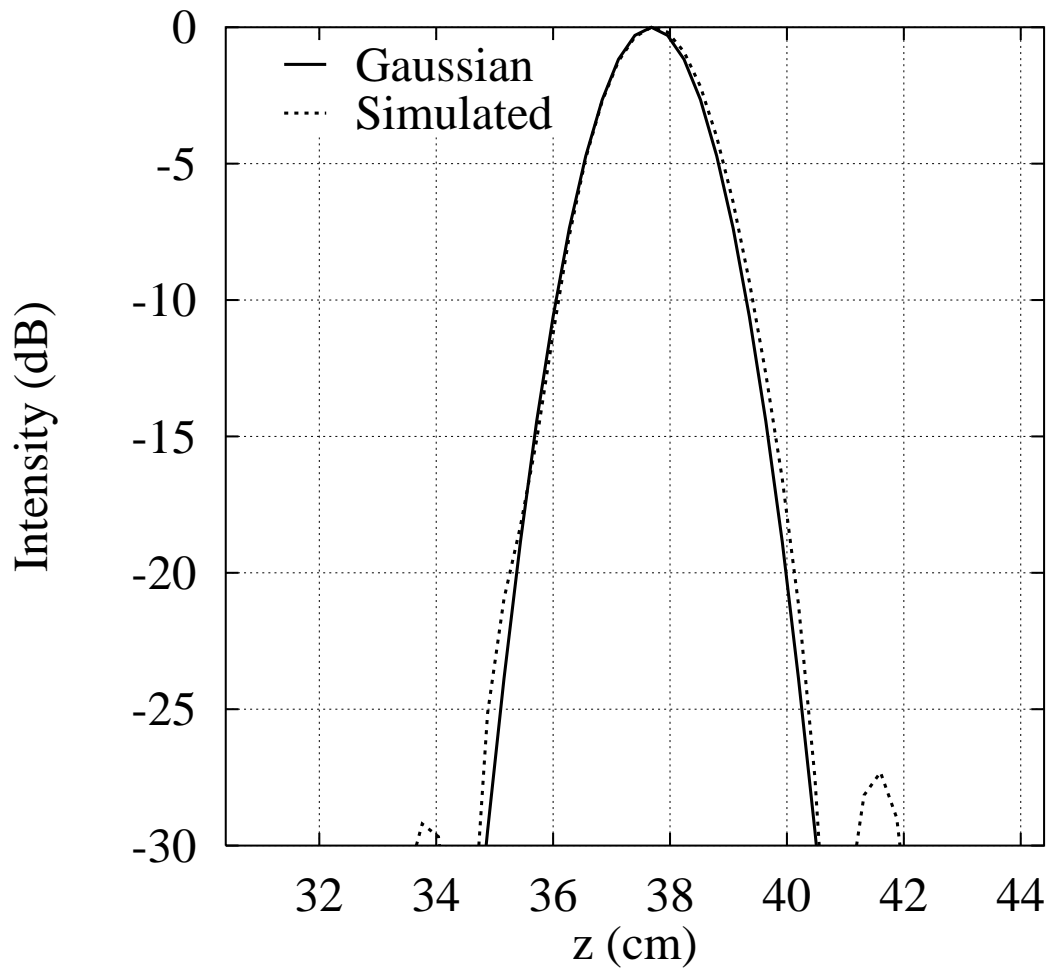
Figure 9: Desired Gaussian (solid) and Simulated (dashed) beam intensities along the *z*-axis at the window plane. The window center is at $z = 37.4$ cm.

5.5 Experimental Results — Cold Tests

The shaped reflectors were fabricated from solid copper and mounted on the feed structure for cold test measurements of the output field. Using the same source/receiver arrangement from the feed field intensity scans (Section 5.2), we measured the output field intensity before, on, and after the window plane. Figure 10 shows the field pattern on the window plane. The measured beam is a well-formed Gaussian with a size, shape, and position that agree well with the simulated beam in Figure 8. The cross-polarized component is approximately 30 dB below the peak of the main polarization, confirming our assumption of a scalar field. The measured beam is slightly elliptical with a waist size in z of 1.6 cm and a waist size in x of 1.7 cm. The larger beam waist of 1.7 cm amounts to only a 0.66λ deviation in beam radius from design. An ideal Gaussian beam with these waist parameters will transmit 99% of the beam power through the 5 cm window aperture; due to the presence of some low sidelobe power, the integrated value for the measured data is 98%. This value is acceptable for high power gyrotron operation, and represents a 1% error in the design. This close agreement of measured beam waist size and transmitted power to the specified design parameters indicate that our reflector shaping approach works very well.

To further examine the Gaussian quality of the beam, we compare an ideal Gaussian intensity profile to that of the measured beam. The measured and theoretical intensity profiles along z are given in Figure 11. We note the measured beam has an excellent Gaussian profile that matches the ideal beam over the range of appreciable intensity. The -21 dB sidelobe to the right of the main beam appears because the sidelobe incident on the third reflector (see Figure 3) is not fully reflected into the main beam. This sidelobe may be unrecoverable because it is propagating at a different angle than the main beam, most likely the result of spurious mode radiation from the launcher.

The Gaussian nature of the beam can also be verified by considering the evolution of the wave profile with distance. Figure 12 shows the beam intensity contours on a plane located 60 cm from the window aperture. The field is Gaussian with a waist size of 3.9 cm in both x and z; the theoretical waist size (assuming a minimum waist at the window of 1.6 cm) is 3.6 cm. This 0.3 cm divergence in beam size over the 60 cm (220λ) propagation distance is practically negligible, and we see that the measured beam behaves as a nearly-ideal Gaussian beam.

We have shown explicitly, using the measured field intensities, that the output beam is a well-formed Gaussian with parameters close to those of the design. We can extend the data analysis by employing the phase retrieval algorithm to round out the study. With input field intensities on planes located 10 cm before, at, and 40 cm beyond the window position in y, we retrieved the phase over the window aperture, and this phase is shown in Figure 13 along the z-axis. Since the design Gaussian beam has its minimum waist at the window, we expect the phase there to be flat. This is indeed the case for the reconstructed output field phase of Figure 13. The mild slope in the phase arises because the beam is propagating at an angle of 0.2^o in the $y-z$ plane, which leads to a small beam-center offset in z (see Figure 12).
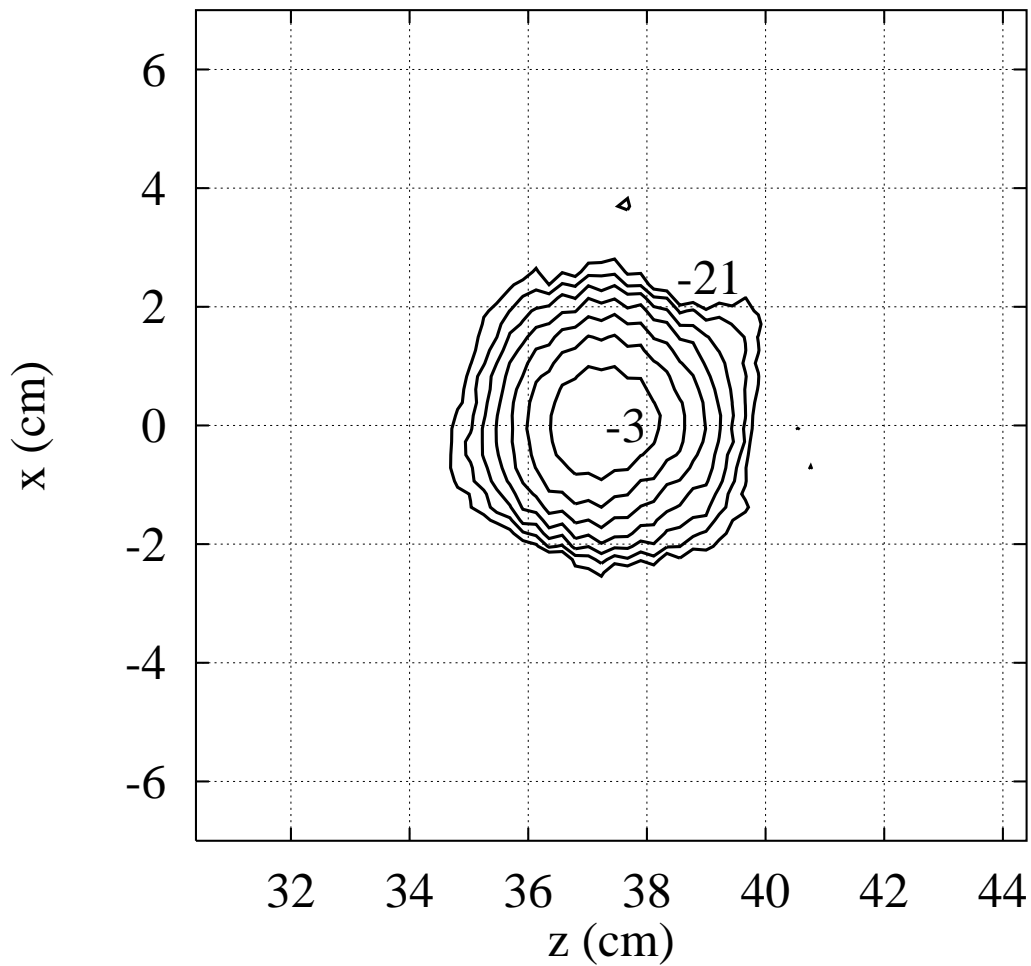
Figure 10: Measured field intensity on the window plane. The window center is at $z = 37.4$ cm, $x = 0$ cm. Contours of constant $|E_x|^2$ are at 3 dB intervals from peak; the -3 dB and -21 dB curves are labeled.
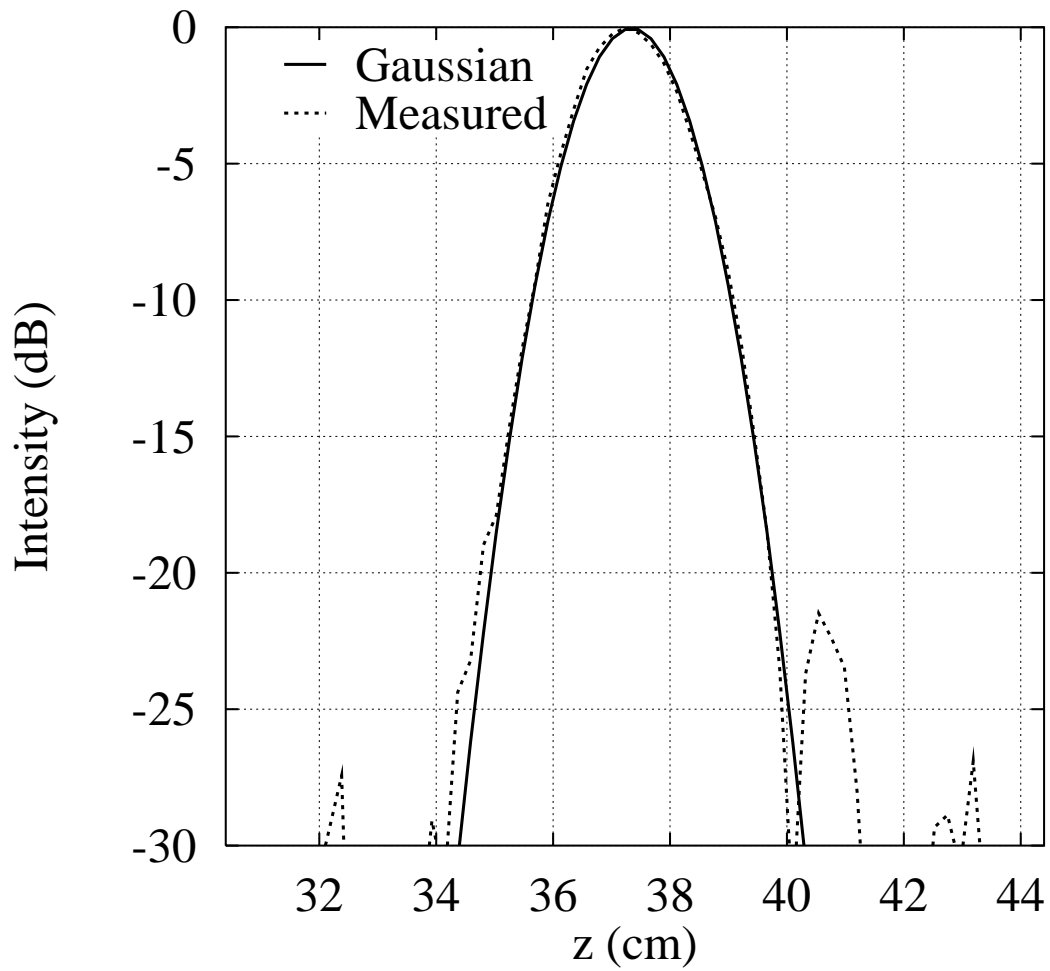
Figure 11: Gaussian beam with a *z*-waist of 1.6 cm (solid) and Measured beam (dashed) intensity along the *z*-axis of the window plane. The window center is at $z = 37.4$ cm.
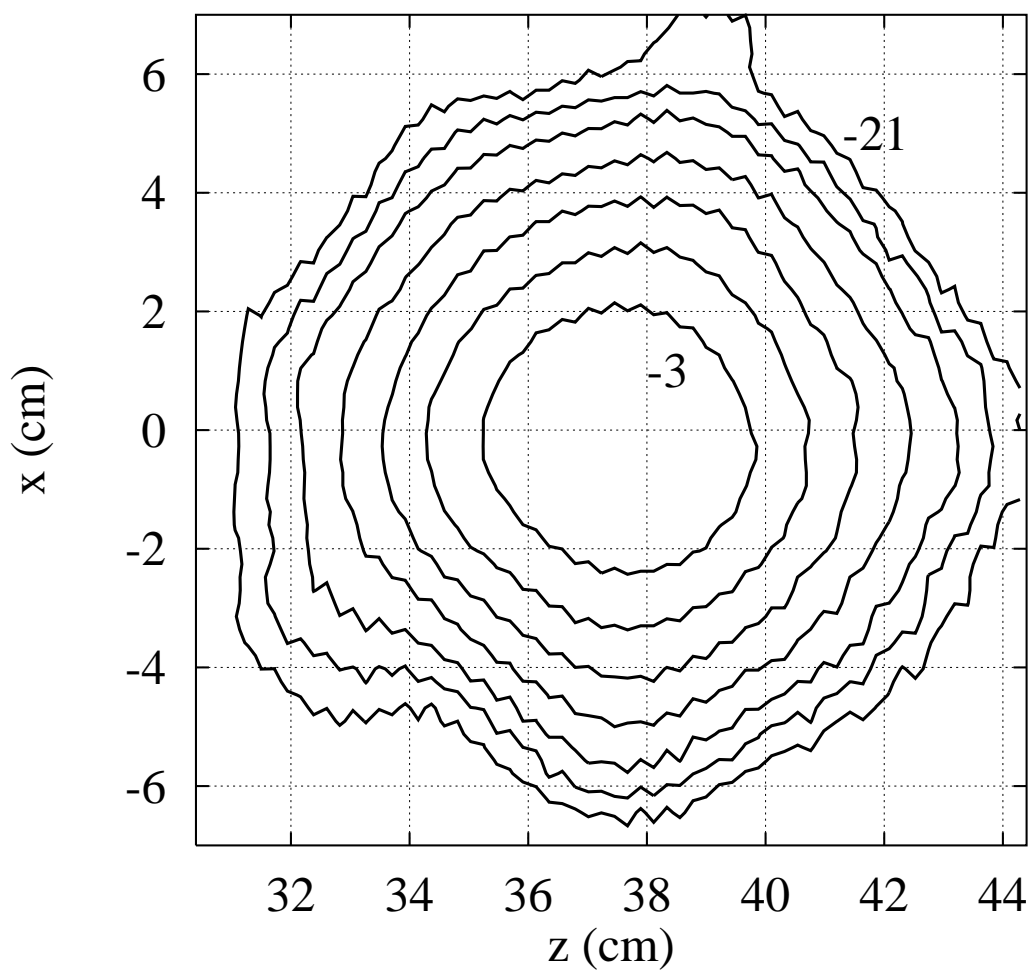
Figure 12: Measured field intensity 60 cm from the window plane. Contours of constant $|E_x|^2$ are at 3 dB intervals from peak; the -3 dB and -21 dB curves are labeled.
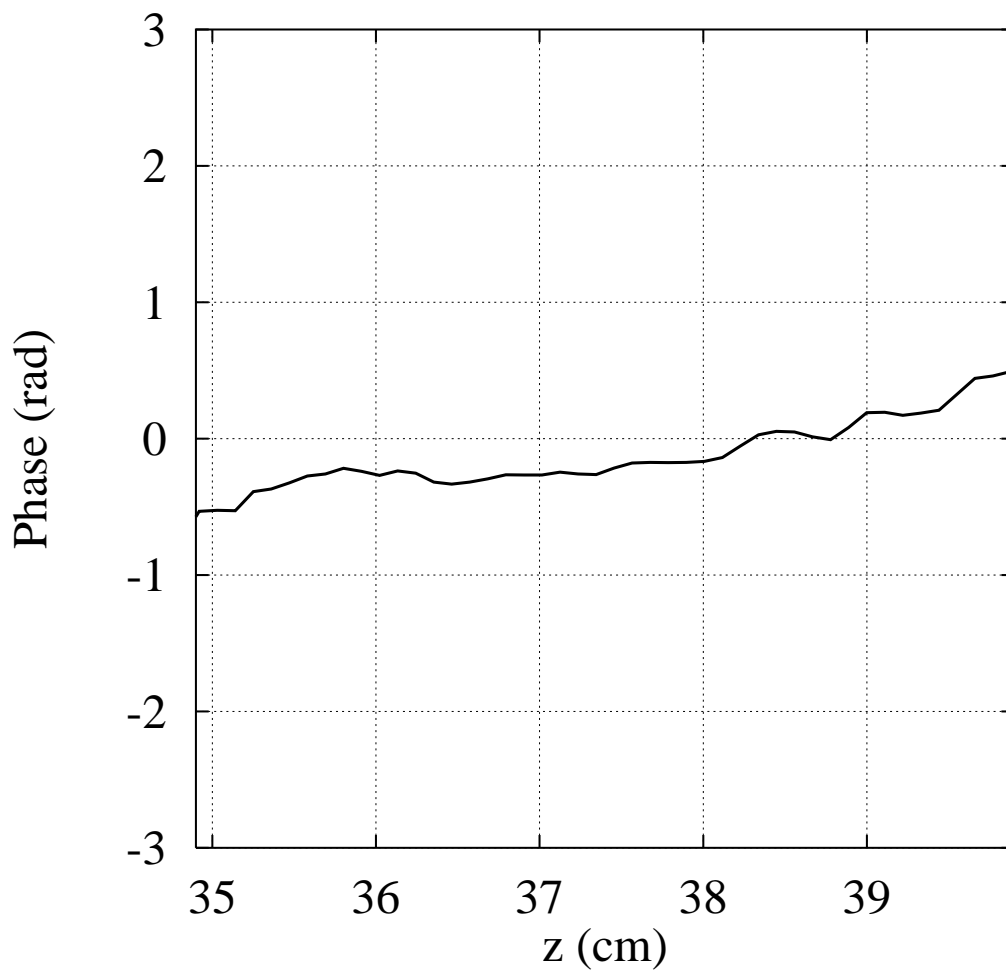
Figure 13: Reconstructed phase of the measured beam over the window aperture along the *z*-axis.

5.6   Experimental Results — Hot Tests

The complete mode converter was assembled and placed inside the gyrotron for hot, or high-power, testing with the diamond window at CPI. The tube operated at 650 kW for 1.6 s pulse lengths and at 940 kW for 0.001 s pulse lengths with an average power of 50 kW. The diamond window performed well throughout the testing, indicating that the microwave beam is well-matched to the window aperture. Preliminary infrared camera measurements were also made that confirm the Gaussian shape of the output beam. Figure 14 shows normalized intensity contours of an IR camera measurement 12.7 cm from the window. The dimensions in Figure 14 are based on estimated beam size at that plane position. The precise size and position of the beam are unknown because of difficulties associated with determining a reference frame in the closed load system. However, we can infer from the Gaussian shape of the intensity contours and the fact that the beam passes through the window with very low loss that the high-power microwave beam has characteristics close to those of the cold test results discussed in Section 5.5.

6   Conclusions

We have presented a general method for designing reflectors in quasi-optical systems based on phase retrieval from intensity-only measurements. The method relies on a fast phase retrieval algorithm that is also used to shape phase-correcting surfaces. Following the basic development of necessary components, we applied the method to the specific case of designing gyrotron internal mode converter reflectors to produce a specified Gaussian beam on the gyrotron vacuum window. The field intensity radiated by the feed (launcher and two toroidal reflectors) was measured and the phase reconstructed from those measurements. The reconstructed wave then served as input to the reflector shaping routine, from which we derived the reflector surface shapes. The reflectors were then mounted in the mode converter and we measured the final output beam. Examination of the output beam parameters showed that the design method works extremely well, producing a beam with a waist size that differed from design by only 0.66λ. We showed that approximately 98% of the power in the beam will exit the window aperture and that beyond the aperture the beam evolves as a nearly-ideal Gaussian with the prescribed flat phase profile at the window plane. High-power testing of the mode converter indicates that the output beam is well-matched to the diamond window, which should enable long-pulse operation of the gyrotron. The experimental validation of the proposed design approach along with its general formulation in terms of quasi-optical phase-correction provide incentive for applying the method to other areas of microwave engineering such as radio astronomy and high-power microwave structure design.

7   Acknowledgements

The authors gratefully acknowledge Dr. Kevin Felch and Dr. Steve Cauffman at Communications and Power Industries for their help in conducting the experiments reported in
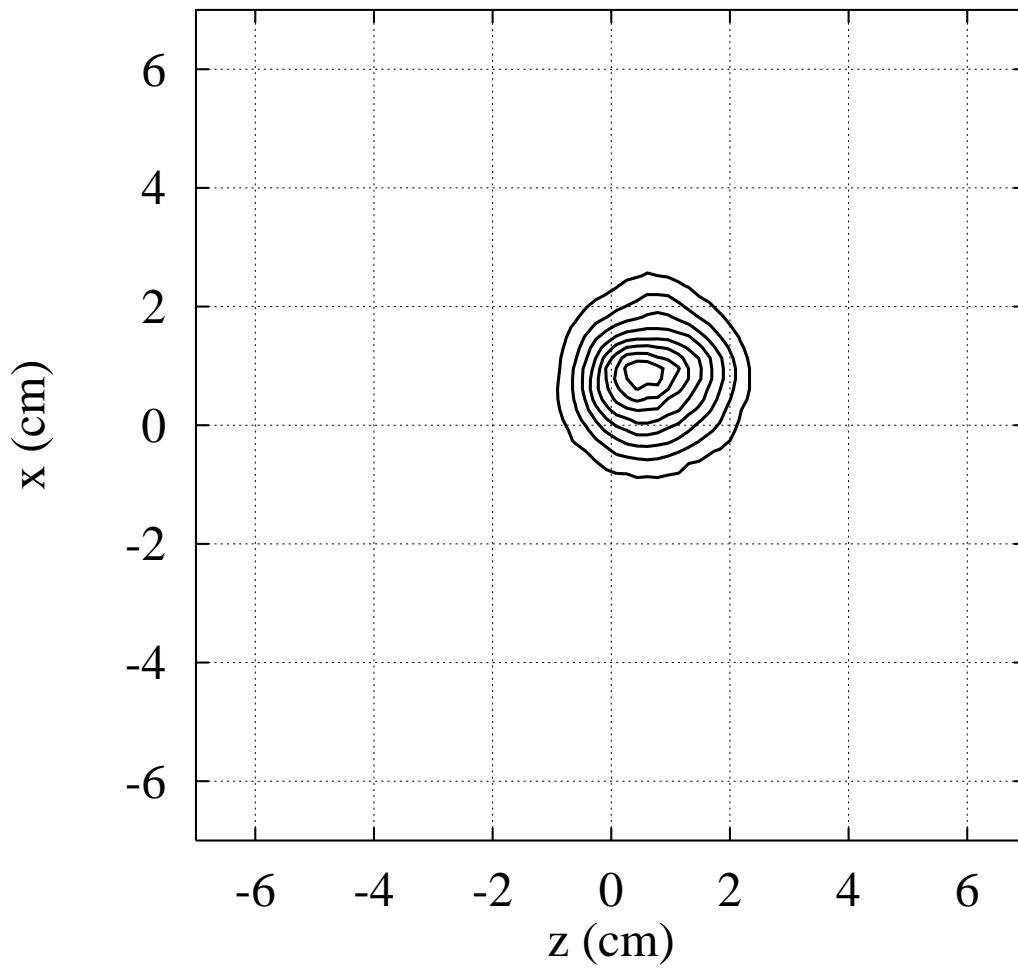
Figure 14: Infrared camera measurement of the gyrotron microwave beam 12.7 cm from the diamond window. Normalized intensity contours are shown at 0.1 increments from peak.

References

[1] S. N. Vlasov, L. I. Zagryadskaya, and M. I. Petelin, "Transformation of a whispering gallery mode, propagating in a circular waveguide, into a beam of waves," *Radio Engineering and Electronic Physics*, vol. 12, no. 10, pp. 14 – 17, 1975.

[2] G. G. Denisov, A. N. Kuftin, V. I. Malygin, N. P. Venediktov, D. V. Vinogradov, and V. E. Zapevelov, "110 GHz gyrotron with built-in high-efficiency converter," *International Journal of Electronics*, vol. 72, no. 5 and 6, pp. 1079–1091, 1992.

[3] M. Blank, K. Kreischer, and R. J. Temkin, "Theoretical and experimental investigation of a quasi-optical mode converter for a 110-GHz gyrotron," *IEEE Transactions on Plasma Science*, vol. 24, no. 3, pp. 1058–1066, 1996.

[4] H. A. Haus, *Waves and Fields in Optoelectronics*. Englewood Cliffs, NJ: Prentice-Hall, 1984.

[5] J. A. Lorbeck and R. J. Vernon, "A shaped-reflector high-power converter for a whispering-gallery mode gyrotron output," *IEEE Transactions on Antennas and Propagation*, vol. 43, pp. 1383 – 1388, Dec. 1995.

[6] K. Felch, M. Blank, P. Borchard, T. S. Chu, J. Feinstein, H. R. Jory, J. A. Lorbeck, C. M. Loring, Y. M. Mizuhara, J. M. Neilson, R. Schumacher, and R. J. Temkin, "Long-pulse and CW tests of a 110-GHz gyrotron with an internal, quasi-optical mode converter," *IEEE Transactions on Plasma Science*, vol. 24, no. 3, pp. 558–569, 1996.

[7] D. R. Denison, T. Kimura, M. A. Shapiro, and R. J. Temkin, "Phase retrieval from gyrotron near-field intensity measurements," in *Conference Digest – Twenty Second International Conference on Infrared and Millimeter Waves*, pp. 81 – 82, 1997.

[8] D. R. Denison, M. A. Shapiro, and R. J. Temkin, "Reflector antenna shaping from feed field intensity measurements," in *Conference Digest – USNC/URSI National Radio Science Meeting*, p. 258, 1998.

[9] B. Z. Katsenelenbaum and V. V. Semenov, "Synthesis of phase correctors shaping a specified field," *Radio Engineering and Electronic Physics*, vol. 12, pp. 223 – 230, 1967.

[10] R. W. Gerchberg and W. O. Saxton, "A practical algorithm for the determination of phase from image and diffraction plane pictures," *Optik*, vol. 35, no. 2, pp. 237 – 246, 1972.

[11] A. P. Anderson and S. Sali, "New possibilities for phaseless microwave diagnostics. Part 1: Error reduction techniques," *IEE Proceedings*, vol. 132, Pt. H, pp. 291 – 298, Aug. 1985.

[12] L. S. Taylor, "The phase retrieval problem," *IEEE Transactions on Antennas and Propagation*, vol. AP-29, pp. 386 – 391, Mar. 1981.

[13] J. R. Fienup, "Phase retrieval algorithms: A comparison," *Applied Optics*, vol. 21, no. 15, pp. 2758 – 2769, 1982.

[14] R. H. T. Bates, "Fourier phase problems are uniquely solvable in more than one dimension. I: Underlying theory," *Optik*, vol. 61, no. 3, pp. 247 – 262, 1982.

[15] A. V. Chirkov, G. G. Denisov, and N. L. Aleksandrov, "3D wavebeam field reconstruction from intensity measurements in a few cross sections," *Optics Communications*, vol. 115, pp. 449 – 452, 1995.

[16] T. Isernia, G. Leone, and R. Pierri, "Radiation pattern evaluation from near-field intensities on planes," *IEEE Transactions on Antennas and Propagation*, vol. 44, pp. 701 – 710, May 1996.

[17] W. H. Press, S. A. Teukolsky, W. T. Vetterling, and B. P. Flannery, *Numerical Recipes in Fortran: The Art of Scientific Computing*. New York: Cambridge University Press, second ed., 1992.

[18] A. A. Bogdashov, A. V. Chirkov, G. G. Denisov, D. V. Vinogradov, A. N. Kuftin, V. I. Malygin, and V. E. Zapevalov, "Mirror synthesis for gyrotron quasi-optical mode converters," *International Journal of Infrared and Millimeter Waves*, vol. 16, no. 4, pp. 735 – 744, 1995.

[19] G. G. Denisov, A. V. Chirkov, D. V. Vinogradov, V. I. Malugin, A. A. Bogdashov, V. I. Belousov, N. L. Alexandrov, and V. E. Zapelov, "Phase corrector synthesis and field measurements for gyrotron quasi-optical wave beams," in *Conference Digest – Twentieth International Conference on Infrared and Millimeter Waves*, pp. 483 – 484, 1995.

[20] Y. Hirata, Y. Mitsunaka, K. Hayashi, and Y. Itoh, "Wave-beam shaping using multiple phase-correction mirrors," *IEEE Transactions on Microwave Theory and Techniques*, vol. 45, pp. 72 – 77, Jan. 1997.

[21] C. P. Moeller, "A coupled cavity whispering gallery mode transducer," in *Conference Digest – Seventeenth International Conference on Infrared and Millimeter Waves*, pp. 42 – 43, 1992.